Biogeosciences, 11, 6107–6117, 2014
www.biogeosciences.net/11/6107/2014/
doi:10.5194/bg-11-6107-2014

Biogeosciences Open Access

Wind-driven changes in the ocean carbon sink

N. C. Swart[1], J. C. Fyfe[1], O. A. Saenko[1], and M. Eby[2]

[1]Canadian Centre for Climate Modelling and Analysis, University of Victoria, P.O. Box 1700 STN CSC, Victoria, BC, V8W 2Y2, Canada
[2]School of Earth and Ocean Sciences, University of Victoria, Victoria, BC, Canada

Correspondence to: N. C. Swart (neil.swart@ec.gc.ca)

Received: 3 April 2014 – Published in Biogeosciences Discuss.: 4 June 2014
Revised: 23 September 2014 – Accepted: 1 October 2014 – Published: 13 November 2014

Abstract. We estimate changes in the historical ocean carbon sink and their uncertainty using an ocean biogeochemical model driven with wind forcing from six different reanalyses and using two different eddy parameterization schemes. First, we quantify wind-induced changes over the extended period from 1871 to 2010 using the 20th Century Reanalysis winds. Consistent with previous shorter-term studies, we find that the wind changes act to reduce the ocean carbon sink, but the wind-induced trends are subject to large uncertainties. One major source of uncertainty is the parameterization of mesoscale eddies in our coarse resolution simulations. Trends in the Southern Ocean residual meridional overturning circulation and the globally integrated surface carbon flux over 1950 to 2010 are about 2.5 times smaller when using a variable eddy transfer coefficient than when using a constant coefficient in this parameterization. A second major source of uncertainty arises from disagreement on historical wind trends. By comparing six reanalyses over 1980 to 2010, we show that there are statistically significant differences in estimated historical wind trends, which vary in both sign and magnitude amongst the products. Through simulations forced with these reanalysis winds, we show that the influence of historical wind changes on ocean carbon uptake is highly uncertain, and the resulting trends depend on the choice of surface wind product.

1 Introduction

Estimates of historical ocean carbon uptake by ocean biogeochemical models are a central constraint in our understanding of the global carbon cycle (Le Quéré et al., 2013; Wanninkhof et al., 2013; Sarmiento et al., 2010). The rate of simulated ocean carbon uptake in such models is sensitive to trends in surface wind forcing, particularly over the Southern Ocean. Several previous ocean model studies, forced at the surface by reanalysis winds, have suggested that the historical intensification of the Southern Hemisphere westerlies has reduced the Southern Ocean CO_2 sink (e.g. Le Quéré et al., 2007; Lovenduski et al., 2007). The intensified winds reduce the CO_2 sink by increasing the Southern Ocean residual overturning circulation and, consequently, the rate of outgassing of natural CO_2 (Lovenduski et al., 2008).

However, large uncertainties exist in previous model-based estimates of the wind feedback on historical ocean carbon uptake. Firstly, the previous studies have primarily used NCEP/NCAR (National Centers for Environmental Prediction/National Center for Atmospheric Research) Reanalysis 1 (R1) to derive the surface wind forcing, limiting them to the period after 1948. The influence of wind changes prior to 1948 remain unknown. Secondly, the wind-induced circulation changes are modulated by ocean eddies (Lovenduski et al., 2013; Böning et al., 2008), which are neither resolved nor adequately parameterized in many studies using coarse resolution models, which have tended to use a constant coefficient of eddy diffusivity (e.g. Le Quéré et al., 2010, 2007; Lovenduski et al., 2008) . Finally, the historical wind changes are themselves uncertain, as evidenced by differences amongst trends over 1980 to 2010 in the available reanalyses (Swart and Fyfe, 2012).

The wind-induced increase in the outgassing of natural CO_2 from the Southern Ocean is also offset by an enhanced uptake of anthropogenic CO_2 driven by the rising atmospheric concentrations, although the question of which process dominates is subject to debate (Le Quéré et al., 2010; Zickfeld et al., 2008). The resulting net trend in historical

Table 1. List of Reanalysis surface winds (speed and stress fields) used in this study. 20CR is an ensemble Reanalysis, and here we have used the ensemble mean. NCEP/DOE = National Centers for Environmental Prediction /Department of Energy; CFSR = Climate Forecast System Reanalysis; MERRA = Modern Era Retrospective Analysis for Research and Applications.

Name	Abbreviation	Reference
NCEP/NCAR Reanalysis 1	R1	Kalnay et al. (1996)
NCEP/DOE Reanalysis 2	R2	Kanamitsu et al. (2002)
20th Century Reanalysis v2	20CR	Compo et al. (2011)
ERA-Interim Reanalysis	ERA-Int	Dee et al. (2011)
NCEP CFSR	CFSR	Saha et al. (2010)
NASA MERRA	MERRA	Rienecker et al. (2011)

Southern Ocean uptake remains uncertain (Lenton et al., 2013), but it is of key interest given the primary importance of the region for anthropogenic CO_2 uptake (Wanninkhof et al., 2013; Gruber et al., 2009).

Here, we work to address the uncertainties in the wind feedback on ocean carbon uptake. We use the 20th Century Reanalysis, version 2 (20CR) (Compo et al., 2011) to produce a model-based estimate of historical ocean carbon uptake since 1871. First, we examine the influence of time evolving wind changes on surface carbon fluxes. Next, we test the sensitivity of the wind-induced changes in circulation and surface fluxes to the type of eddy parameterization. Finally, we show how differences in wind changes among six reanalyses influence the wind feedback on carbon uptake over the period 1980 to 2010.

2 Data and methods

2.1 The UVic Earth System Climate Model

We use version 2.9 of the University of Victoria Earth System Climate Model (UVic ESCM), which is an Earth System Model of intermediate complexity described by Weaver et al. (2001). The UVic ESCM has a fully dynamic 3D ocean general circulation model, coupled to a vertically integrated energy-moisture balance (EMB) atmosphere model and a thermodynamic–dynamic sea ice model (Weaver et al., 2001). All the model components share a global domain with a horizontal resolution of 3.6° longitude by 1.8° latitude, and there are 19 vertical levels in the ocean.

The UVic ESCM also incorporates a state of the art ocean carbon cycle, which simulates interior distributions of dissolved inorganic carbon (DIC) and alkalinity, as well as surface fluxes of CO_2 and historical cumulative ocean carbon uptake that are in good agreement with observations (Eby et al., 2013, 2009; Schmittner et al., 2008).

In the default version of the UVic ESCM, mesoscale ocean eddies are represented via the Gent–McWilliams (GM) eddy parameterization (Gent and McWilliams, 1990), which has a constant eddy transfer coefficient of $800\,\mathrm{m^2\,s^{-1}}$. Here, we have also implemented a variable eddy transfer coefficient. In this formulation, which follows Gnanadesikan et al. (2006) and Farneti and Gent (2011), the GM eddy transfer coefficient is allowed to vary in space and time and is prescribed as

$$K_{\mathrm{GM}}(x,y,t) = \frac{\alpha}{h-h_{\mathrm{m}}} \int_{-h}^{-h_{\mathrm{m}}} |\nabla\rho|\,\mathrm{d}z \left(\frac{gL^2}{\rho_0 N_0}\right), \quad (1)$$

where g is the gravitational acceleration, $\rho_0 = 1025\,\mathrm{kg\,m^{-3}}$ is a constant reference density, N_0 is a prescribed constant buoyancy frequency of $0.004\,\mathrm{s^{-1}}$, L is a constant prescribed eddy length scale of 50 km, α is a dimensionless tuning constant set to 1 and $|\nabla\rho|$ is the horizontal density gradient or baroclinicity, which is averaged over depths between $h_{\mathrm{m}} = 100$ and $h = 2000$ m. The range of K_{GM} is then constrained between a minimum of 300 and a maximum of $5000\,\mathrm{m^2\,s^{-1}}$. For each experiment described below, one version is conducted with the constant GM coefficient and a second version is conducted with the variable GM formulation.

2.2 Experimental design

Due to the simplified nature of the UVic ESCM's atmosphere, ocean surface wind stress and wind speed fields are specified, but the surface buoyancy flux is computed prognostically. The model was equilibrated for over 10 000 years with year 1800 forcing (greenhouse gas, sulphate aerosol, land use, orbital, solar) using surface wind speed and wind stress climatologies derived from the 20CR over the years 1871 to 1899. The 20CR is an ensemble reanalysis, and we use the ensemble mean monthly wind fields. The publicly distributed 20CR ensemble mean wind speeds were incorrectly calculated, but here we use a correctly recalculated ensemble mean.

After the model spin-up, transient simulations were run for the period 1800 to 2010 under historical forcing. Two sets of time evolving runs were conducted under 20CR winds. In the "FIXED" simulations, the radiative forcing evolved in time, but the winds were held fixed by using repeating monthly winds from 1871. In "TRANSIENT" simulations, the winds evolved according to 20CR monthly winds from 1871 onwards. The influence of wind changes on surface CO_2 fluxes is computed as TRANSIENT minus FIXED. In addition, "CONTROL" simulations with fixed winds and pre-industrial radiative forcing were also done and subtracted from the time evolving runs to remove any residual model drift, although the drift is very small due to the long spin-up.

An additional set of simulations was done to compare wind changes in six different reanalyses for the 1980 to 2010 period, during which they all overlap (Table 1). For each reanalysis, the model was run for the period 1800 to 1980 with monthly repeating 1980 winds and evolving radiative forcing. In the year 1980, the simulations were branched into two: the first continued with repeating 1980 winds, whilst,

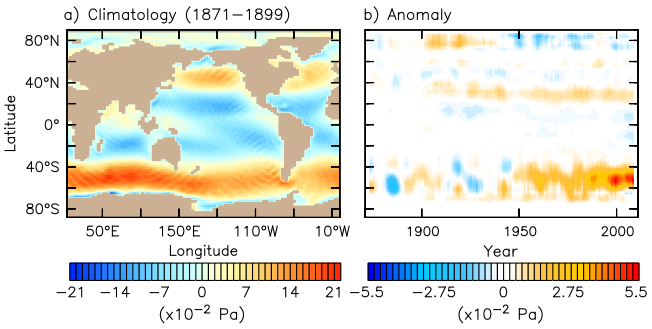

Figure 1. (a) The surface zonal wind stress climatology of 20CR over 1871 to 1899 and **(b)** temporal changes in zonal mean stress relative to the climatology.

for the second, the winds evolved monthly, over time, from 1980 to 2010.

2.3 Trends and significance

We calculate linear least-square trends for the surface wind and CO_2 flux fields. The confidence interval of the trends is calculated from the standard error of the estimate multiplied by the 5 % cutoff value of the Student's t distribution with $n-2$ degrees of freedom, where n is the length of the record. Our confidence intervals and p values for the trends are adjusted to take into account the effect of lag-1 autocorrelation in the regression residuals, (r_1), by adjusting the effective sample size, n_t, to an effective sample size: $n_e = n_t \cdot (1-r_1)/(1+r_1)$ in the calculation of the standard error (Santer et al., 2000). We always reported adjusted confidence intervals and p values, unless explicitly stated. Trends are considered significant if the adjusted p value is less than 0.05.

To determine if trends in two related time series differ significantly, we compute the difference between the two series and test the resulting record for a significant trend. Using the difference between the time series removes interannual variability common to both records, which may otherwise obscure significant differences in the background trend. The null hypothesis being tested is whether differences in treatment of the simulations (e.g. constant versus variable GM scheme) have a significant effect on the resulting trends (Santer et al., 2000).

3 The influence of wind and eddy changes since 1871

3.1 Climatology and changes in 20CR winds

The most prominent trends in the 20CR winds occur in the region of the Southern Hemisphere (SH) westerlies (Fig. 1). In the zonal mean, the SH westerly jet shows variability in its strength up until about 1950, indicated by positive and negative departures from the climatology (Fig. 1b). From around

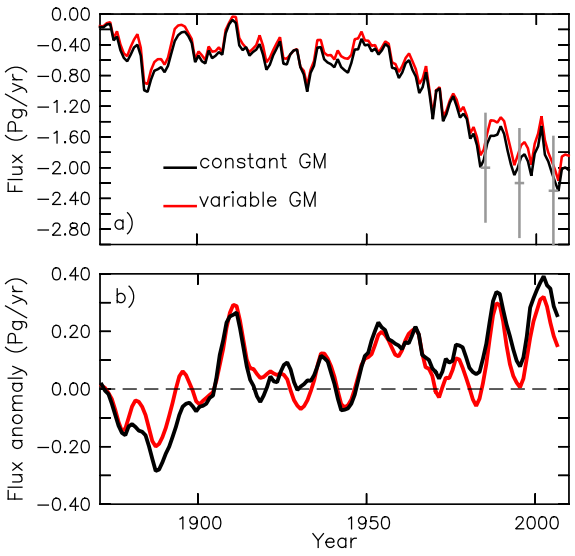

Figure 2. (a) Global net sea–air flux of CO_2 with time-evolving 20CR winds and **(b)** the surface flux anomaly due to the effect of time-evolving winds, computed as the difference between runs with time evolving and fixed winds. Fluxes are positive out of the ocean. The grey bars in **(a)** are observational estimates of the net flux (Ciais et al., 2013).

1950 to 2010, there was also a large intensification of the jet, with the zonal mean stress increasing by about 25 % over this period. This strengthening of the westerly jet is consistent with previous results (Swart and Fyfe, 2012) and is attributable to a combination of ozone and greenhouse gas forcing (Son et al., 2010; Thompson and Solomon, 2002).

We note that uncertainties exist in the 20CR winds, particularly in the Southern Hemisphere during the early part of the reanalysis, when constraining observational data was sparse (Compo et al., 2011). We will consider the effect of wind uncertainty in Sect. 4, but first we will consider the influence of wind changes on surface CO_2 fluxes since 1871 by forcing the UVic ESCM with 20CR winds.

3.2 Changes in surface fluxes and carbon uptake

We first consider the transient simulations which have time-evolving winds and atmospheric CO_2 concentrations that increase according to observations from 283 ppm in 1800 to 379 ppm in 2005 and then following Representative Concentration Pathway 4.5 to 387 ppm in 2010 (Meinshausen et al., 2011). The simulated net sea–air CO_2 flux increases in magnitude in response to these rising atmospheric concentrations (Fig. 2a). The simulated net fluxes fall within observational estimates based on ocean inversions (Khatiwala et al., 2009; Mikaloff Fletcher et al., 2006) for the three decades of the 1980s, 1990s and 2000s (see Ciais et al., 2013, Table 6.1). The fluxes are generally similar, though not identical, in the simulations with a constant and a variable eddy transfer coefficient. The fluxes represent a cumulative

Table 2. Trends in globally integrated net surface CO_2 fluxes (Pg yr^{-1} decade^{-1}). Trends that are statistically significant at the 5 % level are shown in bold (based on an adjusted p value). A negative trend indicates an enhanced ocean carbon sink. Total refers to the net global surface CO_2 flux trend in the simulation. Wind refers to the surface CO_2 flux trend due to wind forcing, calculated as the trend in the transient minus fixed simulation. The 1980–2010 simulations were each done with the variable GM coefficient.

	1871–2010		1950–2010		1980–2010		1990–2010	
Forcing	Total	Wind	Total	Wind	Total	Wind	Total	Wind
1871–2010 simulations								
20CR constant GM	−0.117	0.028	−0.303	0.023	−0.147	0.075	−0.137	0.086
20CR variable GM	−0.111	0.016	−0.279	0.009	−0.135	0.069	−0.142	0.065
1980–2010 simulations								
R1					−0.153	0.102	−0.185	0.123
R2					−0.177	0.112	−0.286	0.064
20CR					−0.237	0.027	−0.304	0.020
ERA-Int					−0.206	0.060	−0.218	0.096
CFSR					−0.318	−0.041	−0.238	0.101
MERRA					−0.319	−0.069	−0.309	−0.010

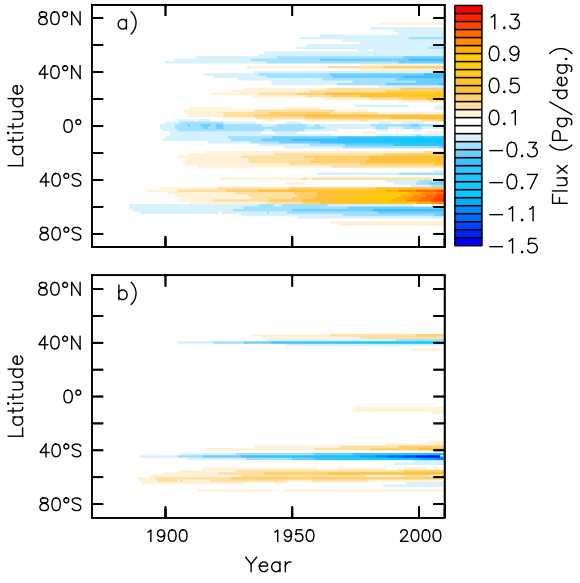

Figure 3. (a) The cumulative zonal mean surface CO_2 flux anomaly over 1871 to 2010 due to the effect of time-evolving winds for the constant GM experiment (transient minus fixed) and **(b)** difference in the flux anomaly between the variable and constant GM experiments. Positive anomalies indicate outgassing.

ocean carbon uptake over 1800 to 2008 of 124 and 112 Pg under the constant and variable GM schemes respectively, which may be compared to the observationally based estimate of 140 ± 25 Pg by Khatiwala et al. (2009). Differences in uptake between the schemes occur because of differences in the mean climate and in the ocean response to changing winds.

Our primary interest lies in the influence of the 20CR wind changes on the net surface CO_2 flux. To consider this, we compute the difference in the net surface fluxes between the transient simulation and the fixed simulation (Fig. 2b). The wind changes result in a negative sea–air CO_2 flux anomaly from 1871 to about 1900, implying an enhanced oceanic carbon sink, which is followed by a brief but large positive anomaly. The flux anomalies over this period are associated with wind variability, particularly the large reduction in zonal wind stress near 60° S which occurred around 1883. The timing of this anomaly is coincident with the eruption of Krakatoa, which may have influenced the winds through aerosol effects. Following this initial variability, the net flux anomaly remained close to zero on average between about 1920 and 1950.

From around 1950 onwards, the wind changes resulted in a net positive sea–air CO_2 flux anomaly, indicating a weakened ocean sink (Fig. 2b), coincident with the intensification of the SH westerlies. Over this period, the wind-induced global flux anomaly becomes about 0.1 Pg yr^{-1} larger in the constant GM scheme than in the variable GM scheme, which is a small difference relative to the interannual variability over the period shown (Fig. 2b). However, the difference in the flux anomalies is significant at the 5 % level, based on a paired sampled t test, and trends in the fluxes differ, as we shall see.

Wind changes reduced the global ocean carbon sink over 1871 to 2010 by 9.5 and 8.3 Pg in the constant and variable GM schemes respectively. The time-cumulative surface fluxes by latitude indicate that the largest CO_2 loss from the ocean due to wind changes occurs in the Southern Ocean between 45 and 60° S under the constant GM scheme (Fig. 3a). It is noteworthy that the outgassing between 45 and 60° S is surrounded by bands of wind-induced ingassing to the north and south. Such compensating changes are also evident in the northern hemisphere between 20 and 60° N, where changes in the Northern Annular Mode and westerly jet (Gillett and Fyfe, 2013) also play a role. In the tropics, changes in the

Table 3. Reduction in the net CO_2 flux due to climate change, over various regions and previous modelling studies in comparison to this work. Where applicable, trends are shown with adjusted confidence intervals. The results from this work come from the 1871 to 2010 simulation using 20CR winds and a constant GM coefficient.

Study and region	Period	Trend Pg yr^{-1} decade^{-1}
Global Ocean		
Le Quéré et al. (2010)	1981–2007	0.12
This study	1981–2007	0.09 ± 0.26
Southern Ocean (> 45° S)		
Le Quéré et al. (2007)	1981–2004	0.018
Lovenduski et al. (2008)	1981–2004	0.07 ± 0.07
This study	1981–2004	0.03 ± 0.07
This study	1950–2010	0.03 ± 0.01

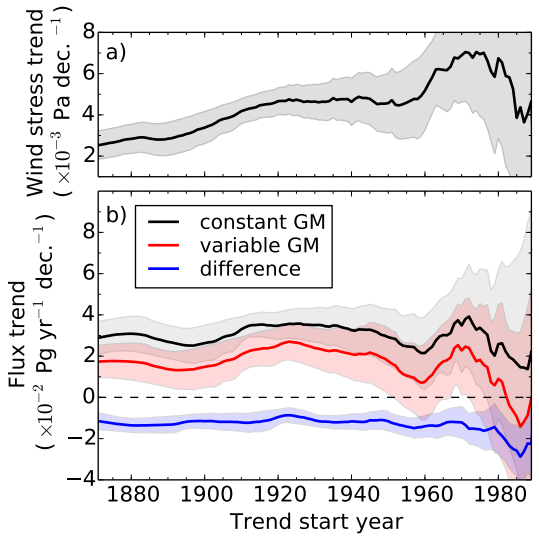

Figure 4. (a) The rolling linear trend in the surface wind stress averaged zonally and over 40–60° S. **(b)** The rolling trend in the Southern Ocean (> 45° S) sea–air CO_2 flux anomaly due to wind changes for the constant and variable GM simulations, as well as the difference in trends between the two. The trends are calculated over the period with a start year, which rolls forward from 1871 to 1990 and an end year of 2010. The solid lines show the trend, and the shaded envelopes are the adjusted 5 to 95 % confidence interval.

trade winds lead to a tripole of fluxes with (relative) ingassing to the south of the equator and outgassing between around 20 to 30° N and S. There are also differences by ocean basin, particularly in the tropics, which are not shown here. The positive globally integrated flux, shown in Fig. 2b, is thus the net result of partial cancellation between regions of large wind-induced ingassing and outgassing, which partly reflects opposing changes between the natural and anthropogenic CO_2 fluxes (Zickfeld et al., 2008). The biggest differences in surface flux between the two eddy schemes also occurs in the Southern Ocean, where there are, again, partially compensating regions of positive and negative anomalies (Fig. 3b).

3.3 Trends in the net global CO_2 fluxes

The trend in the globally integrated surface flux anomaly due to wind changes is 0.023 ± 0.048 Pg yr^{-1} decade^{-1} over 1950 to 2010 under the constant GM scheme (Table 2). For the variable GM scheme, the trend is less than half as large at 0.009 ± 0.052 Pg yr^{-1} decade^{-1} (Table 2). Neither trend is statistically significant at the 5 % level. Global scale trends in the surface CO_2 flux due to historical wind forcing are hard to detect with statistical confidence given the large interannual variability and the partial cancellation of large and opposing regional changes that make up the net global fluxes.

We can detect statistically significant wind-induced trends in the Southern Ocean flux, which are 0.030 ± 0.014 and 0.019 ± 0.016 Pg yr^{-1} decade^{-1} under the constant and variable GM scheme respectively for the period 1950 to 2010 (significant at the 5 % level). Previous modelling studies of about a 25-year duration have reported positive trends in the global and Southern Ocean surface CO_2 flux due to historical wind forcing from NCEP Reanalysis 1 in simulations using a constant coefficient in the GM eddy parameterization. We compare those results with ours in Table 3. Although all simulations give positive trends for the fluxes that are within each other's error bars (where provided), none of the trends are significant at the 5 % level for these short records.

The multidecadal trends are sensitive to the time period selected because of the large interannual variability in the fluxes (Wanninkhof et al., 2013; Lenton et al., 2013), and because the wind speed trend accelerates in time. To see this, we calculated rolling trends over a period with a start year, which rolls forward from 1871 to 1990 and an end year of 2010 (Fig. 4). That is, the trend for 1871 is calculated over 1871 to 2010, while the trend for 1872 is calculated from 1872 to 2010 and so on until 1990. Using the rolling trends, it can be seen that as the Southern Ocean wind speed trends accelerate after 1960 (Fig. 4a), so do the positive trends in the surface flux anomalies. The confidence intervals suggest that significant trends in the surface flux anomaly only emerge above 0 for trends starting before about 1980 (periods > 30 years) under the constant GM scheme and before about 1950 (periods > 60 years) under the variable GM scheme. Conversely, flux anomaly trends based on shorter records are strongly influenced by interannual variability and are not significant. The long timescales required to detect significant trends highlight the value of our long simulations, and we note that, even at the global scale, wind-induced trends are significant over the full record length from 1871 to 2010 (Table 2).

The wind-induced CO_2 flux trends are significantly different between the simulations with the constant and variable GM schemes over the Southern Ocean. The trend in

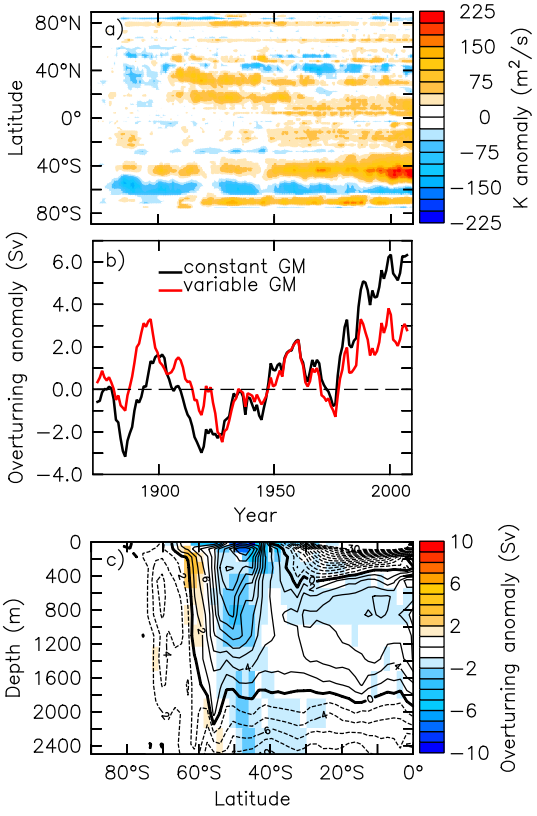

Figure 5. (a) The zonal mean anomaly of eddy diffusivity due to the effect of time-evolving winds in the variable GM experiment (transient minus fixed); **(b)** wind-induced changes in the Southern Ocean residual overturning circulation and **(c)** in shading the difference in the residual overturning stream function between the variable and constant GM experiments with transient winds, averaged over 2000 to 2010, with contours giving the overturning stream function in the constant GM experiment over the same period.

the difference time series between the constant and variable GM fluxes is significant at the 5 % level, regardless of the period over which the trends are calculated (Fig. 4b). This confirms that the surface flux response to wind forcing is fundamentally different between the two schemes. Furthermore, the wind-induced trends in the surface flux also differ significantly between the eddy schemes at the global scale. We now examine the mechanisms behind the differences in the constant and variable GM flux trends.

3.4 Changes in eddies, the meridional overturning circulation and carbon advection

The difference in the zonal mean eddy transfer coefficient between the transient and fixed variable GM simulations shows that the eddy coefficient increased in response to surface wind intensification (Fig. 5a). The most prominent change was an increase in the eddy coefficient in the region between 40 and 50° S, particularly after 1950. The eddy coefficient influences the surface carbon fluxes by modulating the residual overturning circulation. Above topography at the latitudes of the Drake Passage, the Southern Ocean residual meridional overturning stream function can be approximately represented as

$$\Psi_r = -\frac{\tau_x}{\rho f} + K_{\mathrm{GM}} S_b, \tag{2}$$

where τ_x is the zonal wind stress, ρ is the density, f is the Coriolis parameter, K_{GM} is the eddy transfer coefficient and S_b is the slope of isopycnal surfaces (Marshall and Radko, 2003). The first term on the right represents the Eulerian mean (wind driven) circulation and the second term represents the eddy-induced circulation, which tends to oppose the mean flow.

In our simulations, the intensifying westerlies act to increase the rate of the residual overturning circulation through the Eulerian mean component (Fig. 5b). The trend in the residual MOC (Meridional Overturning Circulation) is around 1.0 Sv decade^{-1} (1 Sv = 1 $\times$ 10^6 m^3 s^{-1}) in the constant GM run, where the eddy coefficient is held fixed. In the variable GM simulations, the wind forced trend in the residual MOC is about 2.5 times smaller at 0.37 Sv decade^{-1}. The trend is smaller in the variable scheme because the increase in K_{GM} leads to an increase in the eddy-induced circulation, which partially offsets the changes in the mean component.[1] Spatially, the differing circulation response between the eddy parameterizations occurred principally in the Deacon cell between 40 and 60° S (Fig. 5c).

These changes in the overturning circulation can be connected to changes in the surface carbon flux by considering the DIC budget of the surface of the Southern Ocean for the box south of 45° S and between 0 and 100 m, which is given by

$$\frac{\partial \mathrm{DIC}_{100\,\mathrm{m}}}{\partial t} = J_{\mathrm{adv}} + J_{\mathrm{iso}} + J_{\mathrm{dia}} + J_{\mathrm{gas}} + J_{\mathrm{bio}}, \tag{3}$$

where J_{adv}, J_{iso}, J_{dia}, J_{gas} and J_{bio} represent the fluxes due to Eulerian mean advection, isopycnal mixing arising from parameterized eddies, diapycnal mixing, the sea–air gas exchange and biological processes respectively, as given in Lovenduski et al. (2013). Wind changes increase the surface DIC concentration and lead to the outgassing of CO_2 in both the constant and variable GM experiment, but the changes are greatest with the constant coefficient (6a, b). There is little difference in the biological or diapycnal mixing induced fluxes between the experiments, rather the advective and isopycnal mixing terms are primarily responsible. The isopycnal mixing term associated with the parameterized eddies contains contributions due to along-isopycnal diffusion and due to advection associated with the eddy-induced transport velocities (Gent et al., 1995). The flux of DIC driven by

[1] With a typical isopycnal slope of 10^{-3} and the circumference of the earth at Drake Passage latitudes of 25 $\times$ 10^6 m, a change of K_{GM} of 10^2 m^2 s^{-1} implies a change of eddy-induced overturning of 2.5 Sv, consistent with our model (Fig. 5b).

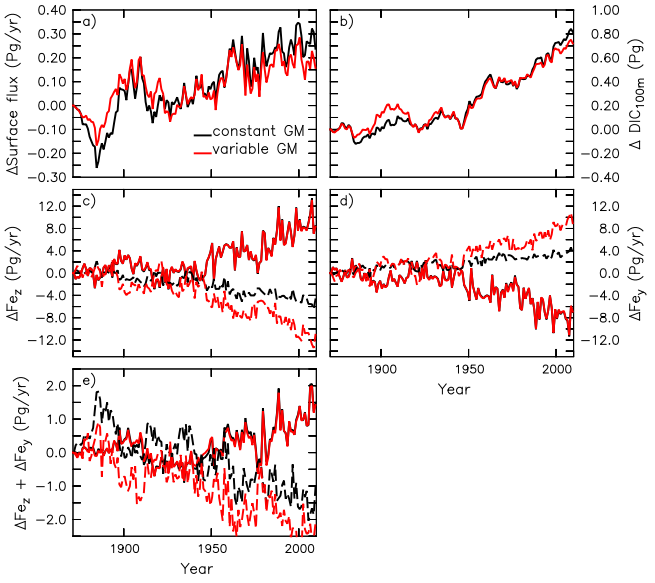

Figure 6. Wind induced effect on **(a)** surface carbon flux south of 45° S, **(b)** DIC inventory integrated south 45° S and over the upper 100 m, **(c)** vertical flux of DIC by Eulerian mean advection (solid lines) and by eddy-induced advection (dashed lines) integrated south 45° S, **(d)** the horizontal components of the DIC advective flux at 45° S and integrated over 0 to 100 m and **(e)** the total advective flux of DIC given by the sum of **(c)** and **(d)**. The wind-induced effect is given by the transient minus fixed experiments, and results are shown for the constant GM (black) and variable GM (red) coefficients.

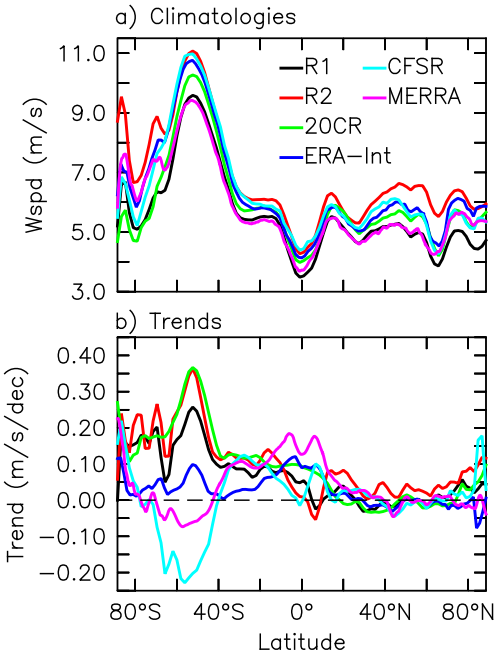

Figure 7. (a) Zonal mean 10 m wind speed climatologies over 1980 to 2010 in six reanalyses and **(b)** zonal mean wind speed trends over the same period. Wind speeds are compared, rather than surface stress fields, because the latter are sensitive to the choice of drag coefficient.

this eddy advection is given by

$$(\mathrm{Fe}_y,\ \mathrm{Fe}_z) = \left(v^* \cdot \mathrm{DIC},\ w^* \cdot \mathrm{DIC}\right), \quad (4)$$

where Fe_y is the horizontal component and Fe_z is the vertical component. There are equivalent terms for the Eulerian mean advection. Wind changes increase vertical advection of DIC into the Southern Ocean surface box by the Eulerian mean circulation (Fig. 6c), representing increased wind-driven upwelling of carbon-rich deep waters. These changes in DIC advection by the mean circulation are basically the same regardless of the GM coefficient. Fluxes due to eddies act in the opposite sense, moving DIC downward out of the surface Southern Ocean. Wind changes also increase this net eddy flux, but the changes are larger under the variable GM scheme because of the increases in K_{GM} (Fig. 6c). There are also compensating changes in horizontal eddy advection of DIC (Fig. 6d), which tends to bring DIC into the Southern Ocean. When summing the vertical and horizontal components, the total effect of eddy-induced advection is to remove DIC from the surface Southern Ocean, and this effect is greater under the variable GM scheme (Fig. 6e). These changes in DIC advection by eddies link the differences in surface CO_2 flux seen between the constant and variable GM simulations directly to the differences in the GM coefficient. There are also indirect effects of differences in the GM scheme, such as changes in sea surface temperature, but the role of K_{GM} driven advection dominates, consistent with Lovenduski et al. (2013).

The mean climate state under the two eddy schemes also differs. In the control simulations with constant pre-industrial wind and radiative forcing, the Southern Ocean residual overturning circulation is 5 Sv or about 25 % weaker under the variable GM scheme, and there are also differences in the Antarctic Circumpolar Current, the subtropical gyres, sea surface temperatures (up to about 0.5 °C on zonal average) and sea ice. These differences in the climate and circulation of the mean state can all affect the surface carbon flux and may also influence the response to changing winds. Nonetheless, even if considered purely in percentage terms relative to the baseline state, changes in the residual overturning circulation shown above are much larger with a constant GM scheme. The partial eddy compensation that occurs in our variable GM simulations is also in agreement with recent theoretical predictions (Meredith et al., 2011), eddy resolving model simulations (Morrison and Hogg, 2012) and other coarse-resolution simulations using a similar variable GM scheme (Lovenduski et al., 2013), which gives us confidence in the robustness of our result. We now turn to the magnitude of the wind forcing itself, which is highly uncertain.

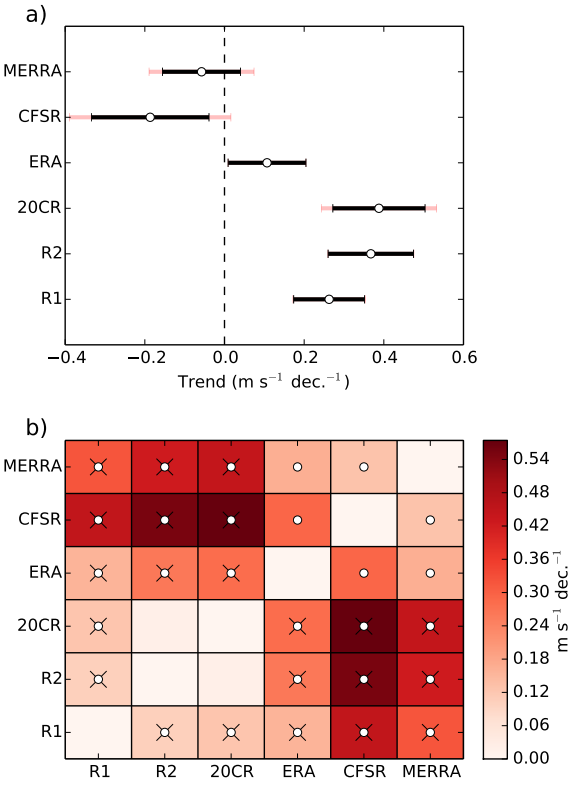

Figure 8. (a) Trends in the 10 m wind speed at the peak of the SH westerly jet over 1980 to 2010 in the six runs forced by reanalysis winds with 95 % confidence intervals in black and adjusted 95 % confidence intervals in red; **(b)** trends of the difference time series in wind speed between all pairwise combinations of the reanalyses are given by the shading. A black "x" indicates that the trends are significantly different at the 5 % level, based on an adjusted p value and a white circle indicates that the trends are significantly different at the 5 % level, based on an unadjusted p value.

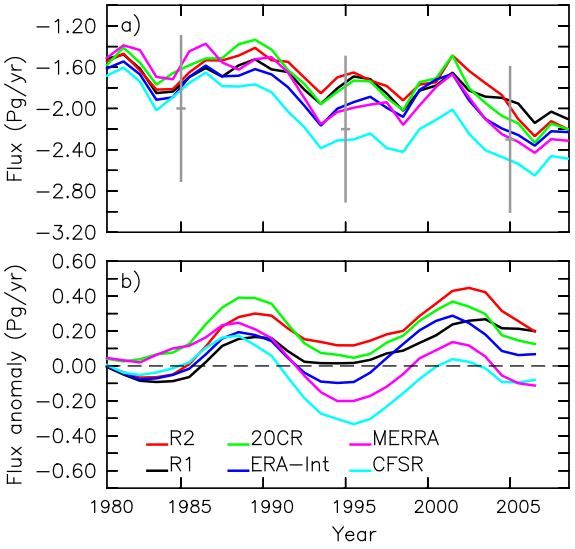

Figure 9. (a) Global net sea–air flux of CO_2 since 1980 for six runs with different reanalysis winds and **(b)** the surface flux anomaly due to the effect of time-evolving winds, computed as the difference between runs with time-evolving and fixed winds. Fluxes are positive out of the ocean. The grey bars in **(a)** are observational estimates of the net flux (Ciais et al., 2013).

4 The oceanic response to wind changes over 1980 to 2010 in six reanalyses

4.1 Comparison of reanalysis winds

To examine the uncertainty in the wind forcing of the ocean, we compare six reanalyses over the period 1980 to 2010 (Table 1). The zonal mean wind speed climatologies show that the reanalyses differ, particularly in the key region of the SH westerlies, which vary in strength by about 20 % amongst the products (Fig. 7a).

The reanalyses also show differences in their surface wind trends over 1980 to 2010 (Fig. 7b). The largest trends generally occur in the SH westerly jets. In that region, the reanalyses do not even agree on the sign of the trend (Fig. 8a). The NASA MERRA (National Aeronautics and Space Administration; Modern Era RetrospectiveAnalysis for Research and Applications) and NCEP CFSR (National Centers for Environmental Prediction; Climate Forecast System Reanalysis) westerly jets have negative trends, which is in disagreement with station based observations and may be due to changes in the type of data assimilated over time (Swart and Fyfe, 2012). Even amongst the remaining four reanalyses that exhibit a positive trend in the SH westerlies, the magnitude of the trends varies by more than three times. To assess the statistical significance of differences in SH jet speed trends between the products, we compute the trend of the difference time series between all possible pairwise combinations of the reanalyses (Fig. 8b). The 20CR and reanalysis 2 (R2) products have statistically indistinguishable trends, but otherwise the trends are significantly different at the 5 % level for almost all possible pairwise comparisons. These uncertainties in the wind climatologies and trends lead to uncertainty in the ocean carbon response, which we now consider.

4.2 The ocean carbon response to different reanalysis winds

We return to considering the net surface CO_2 fluxes, but this time over the period 1980 to 2010, and for six simulations each forced by monthly winds from an individual reanalysis and all using the variable GM scheme (Fig. 9a). Each of these simulations produce a net atmosphere to ocean CO_2 flux within the observational uncertainty (Ciais et al., 2013). The cumulative ocean carbon uptake in these runs by the year 2008 ranges from 119 to 135 Pg due to the differences in the wind forcing, although all are still within the observational estimate of 140 $\pm$ 25 Pg by Khatiwala et al. (2009).

The difference between the simulations with evolving and fixed winds isolates the influence of wind changes on the surface flux (Fig. 9b). The net surface CO_2 fluxes differ significantly at the 5 % level between the runs, based on an analysis of variance and independent sample t tests. The reanalyses with positive trends in the SH westerly jet (R1, R2, 20CR, ERA-Int) show a reduction in the ocean carbon sink, reaching up to 0.11 Pg yr^{-1} decade^{-1} over 1980 to 2010 (Fig. 10a). In contrast, for the other two reanalyses (CFSR, MERRA), the trend is of the opposite sign, indicating enhanced ocean carbon uptake due to historical wind changes, consistent with the large negative and possibly spurious trends in the westerly jets of those reanalysis products. The exact magnitude of the CO_2 flux trends depends on the time frame selected because of the large interannual variability present, but the general conclusion of a large uncertainty amongst products is robust regardless of the choice (Table 2). To test whether the wind-induced flux trends differ in a statistically significant sense, we compute the trend of the difference time series pairwise between each of the six runs (Fig. 10b). The difference trends are significant at the 5 % level for several run combinations, confirming that the flux trends evident in Fig. 9b do differ significantly depending on the choice of forcing product.

The flux trends due to surface wind forcing also depend quantitatively on the experimental design. For example, the 20CR wind-induced trends over 1980 to 2010 differ in the experiment using transient winds over 1871 to 2010 (0.069 Pg yr^{-1} decade^{-1}) compared to the experiment using transient winds over only 1980 to 2010 (0.027 Pg yr^{-1} decade^{-1}). Such a dependency on the onset date of transient winds makes the wind-product comparison experiments reported by Le Quéré et al. (2010) hard to interpret because each of their simulations was initialized at a different time. Our advance here was treating all simulations in a consistent manner over 1800 to 2010, which allows a direct comparison amongst the surface forcing products. The key result is that a large uncertainty exists in the trend of the historical surface of CO_2 flux due to the choice of surface forcing, with a resulting uncertainty of about 16 Pg in the cumulative ocean uptake by 2010.

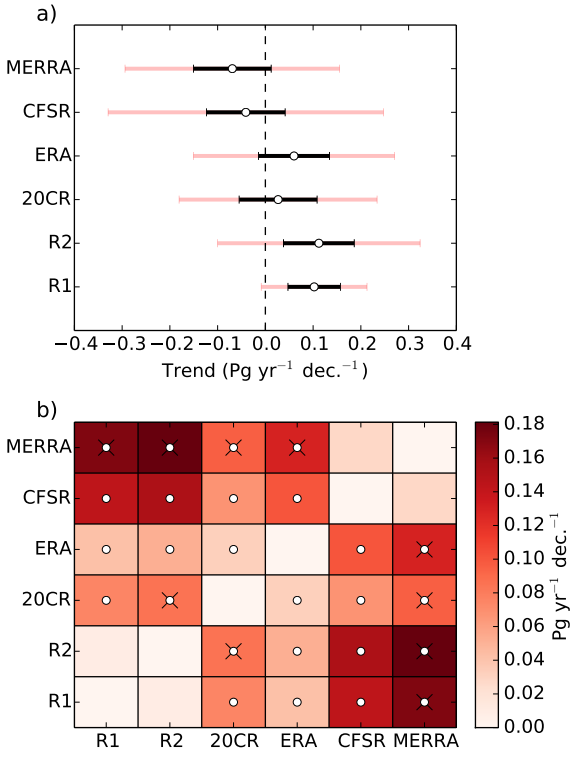

Figure 10. (a) Trends in the net sea–air flux of CO_2 due to wind changes over 1980 to 2010 in the six runs forced by reanalysis winds with 95 % confidence intervals in black and adjusted 95 % confidence intervals in red; **(b)** trends of the difference time series in CO_2 flux between all pairwise combinations of the reanalysis-forced runs are given by the shading. A black "x" indicates that the trends are significantly different at the 5 % level, based on an adjusted p value and a white circle indicates that the trends are significantly different at the 5 % level, based on an unadjusted p value.

5 Conclusions

Using the 20th Century Reanalysis to provide wind forcing, we have produced an ocean biogeochemical model-based estimate of ocean carbon uptake over 1871 to 2010, using both a constant and a variable coefficient in the Gent–McWilliams eddy parameterization scheme. Wind changes led to positive trends in the net sea–air carbon flux, reducing carbon uptake by 8 to 9 Pg, or roughly 10 %, of the total uptake by 2010. However, multidecadal trends were hard to detect with statistical significance due to interannual variability and the partial cancellation of large and opposing regional changes, which make up the net fluxes, particularly at the global scale. At the regional scale south of 45° S, wind-induced surface flux trends could be detected with confidence in our simulations, provided we used a long time period exceeding 30 years. If the historical Southern Ocean wind intensification continues in the future as projected (Swart and Fyfe, 2012), the resulting trends in the surface carbon flux should persist and may become easier to detect in observations, given longer records (Lenton et al., 2013).

The wind effect on ocean circulation and carbon fluxes was dependent on our choice of eddy parameterization. With a variable eddy transfer coefficient, the trend in the Southern Ocean residual overturning circulation and the globally integrated surface carbon flux were about 2.5 times smaller than when using a fixed coefficient. Another source of uncertainty is the significant differences that exist in wind trends from six reanalyses over the period 1980 to 2010. Our simulations indicate that trends in the surface carbon flux depend strongly on the choice of surface wind product.

Acknowledgements. We thank Bill Merryfield and Jim Christian for their helpful comments on the draft manuscript. We acknowledge the computing resources, provided by Westgrid/Compute Canada, which allowed us to conduct the simulations used here.

Edited by: L. Cotrim da Cunha

References

Böning, C., Dispert, A., Visbeck, M., Rintoul, S., and Schwarzkopf, F.: The response of the Antarctic Circumpolar Current to recent climate change, Nat. Geosci., 1, 864–869, doi:10.1038/ngeo362, 2008.

Ciais, P., Sabine, C., Bala, G., Bopp., L., Brovkin, V., Canadell, J., Chhabra, A., DeFries, R., Galloway, J., Heimann, M., Jones, C., Le Quéré, C., Myneni, R., Piao, S., and Thornton, P.: Carbon and Other Biogeochemical Cycles, in: Climate Change 2013: The Physical Science Basis, Contribution of Working Group I to the Fifth Assessment Report of the Intergovernmental Panel on Climate Change, edited by: Stocker, T., Qin, D., Plattner, G.-K., Tignor, M., Allen, S., Boschung, J., Nauels, A., Xia, Y., Bex, V., and Midgley, P., chap. 6, Cambridge University Press, Cambridge, United Kingdom and New York, USA, 2013.

Compo, G. P., Whitaker, J. S., Sardeshmukh, P. D., Matsui, N., Allan, R. J., Yin, X., Gleason, B. E., Vose, R. S., Rutledge, G., Bessemoulin, P., Brönnimann, S., Brunet, M., Crouthamel, R. I., Grant, A. N., Groisman, P. Y., Jones, P. D., Kruk, M. C., Kruger, A. C., Marshall, G. J., Maugeri, M., Mok, H. Y., Nordli, Ø., Ross, T. F., Trigo, R. M., Wang, X. L., Woodruff, S. D., and Worley, S. J.: The Twentieth Century Reanalysis Project, Q. J. Roy. Meteor. Soc., 137, 1–28, doi:10.1002/qj.776, 2011.

Dee, D. P., Uppala, S. M., Simmons, A. J., Berrisford, P., Poli, P., Kobayashi, S., Andrae, U., Balmaseda, M. A., Balsamo, G., Bauer, P., Bechtold, P., Beljaars, A. C. M., van de Berg, L., Bidlot, J., Bormann, N., Delsol, C., Dragani, R., Fuentes, M., Geer, A. J., Haimberger, L., Healy, S. B., Hersbach, H., Hólm, E. V., Isaksen, L., Kållberg, P., Köhler, M., Matricardi, M., McNally, A. P., Monge-Sanz, B. M., Morcrette, J.-J., Park, B.-K., Peubey, C., de Rosnay, P., Tavolato, C., Thépaut, J.-N., and Vitart, F.: The ERA-Interim reanalysis: configuration and performance of the data assimilation system, Q. J. Roy. Meteor. Soc., 137, 553–597, doi:10.1002/qj.828, 2011.

Eby, M., Zickfeld, K., Montenegro, A., Archer, D., Meissner, K. J., and Weaver, A. J.: Lifetime of Anthropogenic Climate Change: Millennial Time Scales of Potential CO_2 and Surface Temperature Perturbations, J. Climate, 22, 2501–2511, 2009.

Eby, M., Weaver, A. J., Alexander, K., Zickfeld, K., Abe-Ouchi, A., Cimatoribus, A. A., Crespin, E., Drijfhout, S. S., Edwards, N. R., Eliseev, A. V., Feulner, G., Fichefet, T., Forest, C. E., Goosse, H., Holden, P. B., Joos, F., Kawamiya, M., Kicklighter, D., Kienert, H., Matsumoto, K., Mokhov, I. I., Monier, E., Olsen, S. M., Pedersen, J. O. P., Perrette, M., Philippon-Berthier, G., Ridgwell, A., Schlosser, A., Schneider von Deimling, T., Shaffer, G., Smith, R. S., Spahni, R., Sokolov, A. P., Steinacher, M., Tachiiri, K., Tokos, K., Yoshimori, M., Zeng, N., and Zhao, F.: Historical and idealized climate model experiments: an intercomparison of Earth system models of intermediate complexity, Clim. Past, 9, 1111–1140, doi:10.5194/cp-9-1111-2013, 2013.

Farneti, R. and Gent, P. R.: The effects of the eddy-induced advection coefficient in a coarse-resolution coupled climate model, Ocean Model., 39, 135–145, doi:10.1016/j.ocemod.2011.02.005, 2011.

Gent, P. and McWilliams, J.: Isopycnal mixing in ocean circulation models, J. Phys. Oceanogr., 20, 150–155, doi:10.1175/1520-0485(1990)020<0150:IMIOCM>2.0.CO;2, 1990.

Gent, P., Willebrand, J., McDougall, T. J., and McWilliams, J.: Parameterizing Eddy-induced tracer transports in Ocean circulation models, J. Phys. Oceanogr., 25, 463–474, doi:10.1175/1520-0485(1995)025<0463:PEITTI>2.0.CO;2, 1995.

Gillett, N. P. and Fyfe, J. C.: Annular mode changes in the CMIP5 simulations, Geophys. Res. Lett., 40, 1189–1193, doi:10.1002/grl.50249, 2013.

Gnanadesikan, A., Dixon, K. W., Griffies, S. M., Balaji, V., Barreiro, M., Beesley, J. A., Cooke, W. F., Delworth, T. L., Gerdes, R., Harrison, M. J., Held, I. M., Hurlin, W. J., Lee, H.-C., Liang, Z., Nong, G., Pacanowski, R. C., Rosati, A., Russell, J., Samuels, B. L., Song, Q., Spelman, M. J., Stouffer, R. J., Sweeney, C. O., Vecchi, G., Winton, M., Wittenberg, A. T., Zeng, F., Zhang, R., and Dunne, J. P.: GFDL's CM2 Global Coupled Climate Models. Part II: The Baseline Ocean Simulation, J. Climate, 19, 675–697, doi:10.1175/JCLI3630.1, 2006.

Gruber, N., Gloor, M., Mikaloff Fletcher, S., Doney, S., Dutkiewicz, S., Follows, M., Gerber, M., Jacobson, A., Joos, F., Lindsay, K., Menemenlis, D., Mouchet, A., Muller, S., Sarmiento, J., and Takahashi, T.: Oceanic sources, sinks, and transport of atmospheric CO_2, Global Biogeochem. Cy., 23, GB1005, doi:10.1029/2008GB003349, 2009.

Kalnay, E., Kanamitsu, M., Kistler, R., Collins, W., Deaven, D., Gandin, L., Iredell, M., Saha, S., White, G., Woollen, J., Zhu, Y., Leetmaa, A., Reynolds, R., Chelliah, M., Ebisuzaki, W., Higgins, W., Janowiak, J., Mo, K. C., Ropelewski, C., Wang, J., Jenne, R., and Joseph, D.: The NCEP/NCAR 40-Year Reanalysis Project, B. Am. Meteorol. Soc., 77, 437–471, doi:10.1175/1520-0477(1996)077<0437:TNYRP>2.0.CO;2, 1996.

Kanamitsu, M., Ebisuzaki, W., Woollen, J., Yang, S.-K., Hnilo, J. J., Fiorino, M., and Potter, G. L.: NCEP–DOE AMIP-II Reanalysis (R-2), B. Am. Meteorol. Soc., 83, 1631–1643, doi:10.1175/BAMS-83-11-1631, 2002.

Khatiwala, S., Primeau, F., and Hall, T.: Reconstruction of the history of anthropogenic CO_2 concentrations in the ocean, Nature, 462, 346–349, doi:10.1038/nature08526, 2009.

Le Quéré, C., Rödenbeck, C., Buitenhuis, E. T., Conway, T. J., Langenfelds, R., Gomez, A., Labuschagne, C., Ramonet, M., Nakazawa, T., Metzl, N., Gillett, N., and Heimann, M.: Saturation of the Southern Ocean CO_2 Sink Due to Recent Climate Change, Science, 316, 1735–1738, doi:10.1126/science.1136188, 2007.

Le Quéré, C., Takahashi, T., Buitenhuis, E. T., Rödenbeck, C., and Sutherland, S. C.: Impact of climate change and variability on the global oceanic sink of CO_2, Global Biogeochem. Cy., 24, GB4007, doi:10.1029/2009GB003599, 2010.

Le Quéré, C., Andres, R. J., Boden, T., Conway, T., Houghton, R. A., House, J. I., Marland, G., Peters, G. P., van der Werf, G. R., Ahlström, A., Andrew, R. M., Bopp, L., Canadell, J. G., Ciais, P., Doney, S. C., Enright, C., Friedlingstein, P., Huntingford, C., Jain, A. K., Jourdain, C., Kato, E., Keeling, R. F., Klein Goldewijk, K., Levis, S., Levy, P., Lomas, M., Poulter, B., Raupach,

M. R., Schwinger, J., Sitch, S., Stocker, B. D., Viovy, N., Zaehle, S., and Zeng, N.: The global carbon budget 1959–2011, Earth Syst. Sci. Data, 5, 165–185, doi:10.5194/essd-5-165-2013, 2013.

Lenton, A., Tilbrook, B., Law, R. M., Bakker, D., Doney, S. C., Gruber, N., Ishii, M., Hoppema, M., Lovenduski, N. S., Matear, R. J., McNeil, B. I., Metzl, N., Mikaloff Fletcher, S. E., Monteiro, P. M. S., Rödenbeck, C., Sweeney, C., and Takahashi, T.: Sea-air CO_2 fluxes in the Southern Ocean for the period 1990–2009, Biogeosciences, 10, 4037–4054, doi:10.5194/bg-10-4037-2013, 2013.

Lovenduski, N. S., Gruber, N., Doney, S. C., and Lima, I. D.: Enhanced CO_2 outgassing in the Southern Ocean from a positive phase of the Southern Annular Mode, Global Biogeochem. Cy., 21, GB2026, doi:10.1029/2006GB002900, 2007.

Lovenduski, N. S., Gruber, N., and Doney, S. C.: Toward a mechanistic understanding of the decadal trends in the Southern Ocean carbon sink, Global Biogeochem. Cy., 22, GB3016, doi:10.1029/2007GB003139, 2008.

Lovenduski, N. S., Long, M. C., Gent, P. R., and Lindsay, K.: Multi-decadal trends in the advection and mixing of natural carbon in the Southern Ocean, Geophys. Res. Lett., 40, 139–142, 2013.

Marshall, J. and Radko, T.: Residual-mean solutions for the Antarctic Circumpolar Current and its associated overturning circulation, J. Phys. Oceanogr., 33, 2341–2354, doi:10.1175/1520-0485(2003)033<2341:RSFTAC>2.0.CO;2, 2003.

Meinshausen, M., Smith, S. J., Calvin, K., Daniel, J. S., Kainuma, M. L. T., Lamarque, J.-F., Matsumoto, K., Montzka, S. A., Raper, S. C. B., Riahi, K., Thomson, A., Velders, G. J. M., and Vuuren, D. P. P.: The RCP greenhouse gas concentrations and their extensions from 1765 to 2300, Climatic Change, 109, 213–241, doi:10.1007/s10584-011-0156-z, 2011.

Meredith, M. P., Naveira Garabato, A. C., Hogg, A. M., and Farneti, R.: Sensitivity of the Overturning Circulation in the Southern Ocean to Decadal Changes in Wind Forcing, J. Climate, 25, 99–110, doi:10.1175/2011JCLI4204.1, 2011.

Mikaloff Fletcher, S. E., Gruber, N., Jacobson, A. R., Doney, S. C., Dutkiewicz, S., Gerber, M., Follows, M., Joos, F., Lindsay, K., Menemenlis, D., Mouchet, A., Müller, S. A., and Sarmiento, J. L.: Inverse estimates of anthropogenic CO_2 uptake, transport, and storage by the ocean, Global Biogeochem. Cy., 20, GB2002, doi:10.1029/2005GB002530, 2006.

Morrison, A. k. and Hogg, A. M.: On the Relationship between Southern Ocean Overturning and ACC Transport, J. Phys. Oceanogr., 43, 140–148, doi:10.1175/JPO-D-12-057.1, 2012.

Rienecker, M. M., Suarez, M. J., Gelaro, R., Todling, R., Bacmeister, J., Liu, E., Bosilovich, M. G., Schubert, S. D., Takacs, L., Kim, G.-K., Bloom, S., Chen, J., Collins, D., Conaty, A., da Silva, A., Gu, W., Joiner, J., Koster, R. D., Lucchesi, R., Molod, A., Owens, T., Pawson, S., Pegion, P., Redder, C. R., Reichle, R., Robertson, F. R., Ruddick, A. G., Sienkiewicz, M., and Woollen, J.: MERRA: NASA's Modern-Era Retrospective Analysis for Research and Applications, J. Climate, 24, 3624–3648, doi:10.1175/JCLI-D-11-00015.1, 2011.

Saha, S., Moorthi, S., Pan, H.-L., Wu, X., Wang, J., Nadiga, S., Tripp, P., Kistler, R., Woollen, J., Behringer, D., Liu, H., Stokes, D., Grumbine, R., Gayno, G., Wang, J., Hou, Y.-T., Chuang, H.-Y., Juang, H.-M. H., Sela, J., Iredell, M., Treadon, R., Kleist, D., Van Delst, P., Keyser, D., Derber, J., Ek, M., Meng, J., Wei, H., Yang, R., Lord, S., Van Den Dool, H., Kumar, A., Wang, W., Long, C., Chelliah, M., Xue, Y., Huang, B., Schemm, J.-K., Ebisuzaki, W., Lin, R., Xie, P., Chen, M., Zhou, S., Higgins, W., Zou, C.-Z., Liu, Q., Chen, Y., Han, Y., Cucurull, L., Reynolds, R. W., Rutledge, G., and Goldberg, M.: The NCEP Climate Forecast System Reanalysis, B. Am. Meteorol. Soc., 91, 1015–1057, doi:10.1175/2010BAMS3001.1, 2010.

Santer, B., Wigley, T., Boyle, J., Gaffen, D., Hnilo, J., Nychka, D., Parker, D., and Taylor, K. E.: Statistical significance of trends and trend differences in layer-average atmospheric temperature time series, J. Geophys. Res., 105, 7337–7356, doi:10.1029/1999JD901105, 2000.

Sarmiento, J. L., Gloor, M., Gruber, N., Beaulieu, C., Jacobson, A. R., Mikaloff Fletcher, S. E., Pacala, S., and Rodgers, K.: Trends and regional distributions of land and ocean carbon sinks, Biogeosciences, 7, 2351–2367, doi:10.5194/bg-7-2351-2010, 2010.

Schmittner, A., Oschlies, A., Matthews, H. D., and Galbraith, E. D.: Future changes in climate, ocean circulation, ecosystems, and biogeochemical cycling simulated for a business-as-usual CO_2 emission scenario until year 4000 AD, Global Biogeochem. Cy., 22, GB1013, doi:10.1029/2007GB002953, 2008.

Son, S.-W., Gerber, E. P., Perlwitz, J., Polvani, L. M., Gillett, N. P., Seo, K.-H., Eyring, V., Shepherd, T. G., Waugh, D., Akiyoshi, H., Austin, J., Baumgaertner, A., Bekki, S., Braesicke, P., Brühl, C., Butchart, N., Chipperfield, M. P., Cugnet, D., Dameris, M., Dhomse, S., Frith, S., Garny, H., Garcia, R., Hardiman, S. C., Jöckel, P., Lamarque, J. F., Mancini, E., Marchand, M., Michou, M., Nakamura, T., Morgenstern, O., Pitari, G., Plummer, D. A., Pyle, J., Rozanov, E., Scinocca, J. F., Shibata, K., Smale, D., Teyssèdre, H., Tian, W., and Yamashita, Y.: Impact of stratospheric ozone on Southern Hemisphere circulation change: A multimodel assessment, J. Geophys. Res.-Atmos., 115, D00M07, doi:10.1029/2010JD014271, 2010.

Swart, N. C. and Fyfe, J. C.: Observed and simulated changes in the Southern Hemisphere surface westerly wind-stress, Geophys. Res. Lett., 39, L16711, doi:10.1029/2012GL052810, 2012.

Thompson, D. W. J. and Solomon, S.: Interpretation of Recent Southern Hemisphere Climate Change, Science, 296, 895–899, doi:10.1126/science.1069270, 2002.

Wanninkhof, R., Park, G. -H., Takahashi, T., Sweeney, C., Feely, R., Nojiri, Y., Gruber, N., Doney, S. C., McKinley, G. A., Lenton, A., Le Quéré, C., Heinze, C., Schwinger, J., Graven, H., and Khatiwala, S.: Global ocean carbon uptake: magnitude, variability and trends, Biogeosciences, 10, 1983–2000, doi:10.5194/bg-10-1983-2013, 2013.

Weaver, A., Eby, M., Wiebe, C., Bitz, M., Duffy, C., Ewen, T., Fanning, A., Holland, M., MacFadyen, A., Matthews, H., Meissner, K., Saenko, O., Schmittner, A., Wang, H., and Yoshimori, M.: The UVic Earth System Climate Model: Model Description, Climatology, and Applications to Past, Present and Future Climates, Atmos. Ocean, 39, 1–68, doi:10.1080/07055900.2001.9649686, 2001.

Zickfeld, K., Fyfe, J., Eby, M., and Weaver, A.: Comment on "Saturation of the Southern Ocean CO_2 Sink Due to Recent Climate Change", Science, 319, 570, doi:10.1126/science.1146886, 2008.